

Random gauge models of the superconductor-insulator transition in two-dimensional disordered superconductors

Enzo Granato

Laboratório Associado de Sensores e Materiais, Instituto Nacional de Pesquisas Espaciais, 12227-010 São José dos Campos, SP, Brazil

(Received 8 August 2017; revised manuscript received 3 November 2017; published 13 November 2017)

We study numerically the superconductor-insulator transition in two-dimensional inhomogeneous superconductors with gauge disorder, described by four different quantum rotor models: a gauge glass, a flux glass, a binary phase glass, and a Gaussian phase glass. The first two models describe the combined effect of geometrical disorder in the array of local superconducting islands and a uniform external magnetic field, while the last two describe the effects of random negative Josephson-junction couplings or π junctions. Monte Carlo simulations in the path-integral representation of the models are used to determine the critical exponents and the universal conductivity at the quantum phase transition. The gauge- and flux-glass models display the same critical behavior, within the estimated numerical uncertainties. Similar agreement is found for the binary and Gaussian phase-glass models. Despite the different symmetries and disorder correlations, we find that the universal conductivity of these models is approximately the same. In particular, the ratio of this value to that of the pure model agrees with recent experiments on nanohole thin-film superconductors in a magnetic field, in the large disorder limit.

DOI: [10.1103/PhysRevB.96.184510](https://doi.org/10.1103/PhysRevB.96.184510)

I. INTRODUCTION

Models of phase coherence in inhomogeneous superconductors, which incorporate gauge disorder, have been widely used to study the vortex glass transition of type-II superconductors driven by thermal fluctuations [1,2]. Gauge disorder appears as random phase shifts in the Josephson junction coupling local superconducting islands due to the combined effect of geometrical disorder and the applied magnetic field. Phase shifts can also arise from the presence of negative Josephson couplings or π junctions [3–5], even in the absence of the magnetic field, and can lead to different phase transitions and changes in the magnetic properties [6–9]. Although there are many recent studies of the effects of disorder both in two-dimensional and one-dimensional [10–12] systems, the superconductor to insulator (SI) transition described by the quantum version of random gauge models has been, to a certain extent, much less investigated [13–16]. The magnetic-field-induced SI transition in thin films has actually been studied in detail using disordered Bose-Hubbard models [17,18], which include a random potential, but the additional effects of gauge disorder are difficult to be included in the numerical simulations [19]. There are, however, interesting superconducting systems in the form of thin films with a pattern of nanoholes [20–25] and microfabricated Josephson-junction arrays [26–29], where gauge disorder alone should play a dominant effect in the properties of the SI transition. Such systems allow comparisons with the results from minimal random gauge models.

Very recently [24,25], the effect of a controlled amount of gauge disorder on the SI transition was investigated in nanohole ultrathin films by introducing geometrical disorder in the form of randomness in the positions of the nanoholes. A minimal model describing phase coherence in these systems consists of a Josephson-junction array defined on an appropriate lattice, with the nanoholes corresponding to the dual lattice [16,30,31]. Positional disorder of the grains or in the plaquette areas [14,32–34] leads to disorder in the magnetic flux per plaquette, which increases with the applied field and geo-

metrical disorder strength. Magnetoresistance oscillations near the SI transition, resulting from commensurate vortex-lattice states, are observed below a critical disorder strength [24]. While the resistivity at the successive field-induced transitions varies below this critical disorder, it reaches a constant value, independent of the critical coupling for larger disorder [25]. Recent numerical simulations of a Josephson-junction array model suggest that the large disorder regime should correspond to a vortex glass [16]. Random gauge models with quantum fluctuations (quantum rotor models) should then provide the simplest description for the SI transition in this limit. Since the choice of the appropriate model is not unique, it should be of interest to compare the results for different models.

In this work, we study numerically the SI transition in two-dimensional inhomogeneous superconductors described by random gauge models. Four different quantum rotor models are considered: a gauge glass, a flux glass, a binary phase glass, and a Gaussian phase glass. The first two models describe the combined effect of geometrical disorder in the array of local superconducting islands and a uniform external magnetic field while the last two describe the effects of randomness in the Josephson couplings alone, allowing for negative couplings. Monte Carlo simulations in the path-integral representation are used to determine the critical exponents and the electrical conductivity at the transition. We find that the gauge- and flux-glass models display the same critical behavior, within the estimated numerical uncertainties. Similar agreement is found for the binary and Gaussian phase-glass models. Despite the different symmetries and disorder correlations, the universal conductivity of these models is approximately the same. We compare the results for gauge- and flux-glass models with recent experiments on nanohole thin-film superconductors in a magnetic field with controlled amount of gauge disorder [24,25]. In particular, the ratio of the critical conductivity for large gauge disorder to that of the pure model is in good agreement with the experimental data. The results support the experimental observation [25] that the critical conductivity is independent of the coupling constant for large disorder, consistent with the scenario of a universal value in this limit.

II. MODELS AND MONTE CARLO SIMULATION

We consider models which describe two-dimensional superconductors as an array of Josephson junctions, allowing for charging effects and gauge disorder [14,16,28,32,35], defined by the Hamiltonian

$$\mathcal{H} = \frac{E_C}{2} \sum_i n_i^2 - \sum_{\langle ij \rangle} E_{ij} \cos(\theta_i - \theta_j - A_{ij}). \quad (1)$$

The first term in Eq. (1) describes quantum fluctuations induced by the charging energy, $E_C n_i^2/2$, of a non-neutral superconducting “grain,” or “island,” located at site i of a reference square lattice, where $E_C = 4e^2/C$, e is the electronic charge, and $n_i = -i\partial/\partial\theta_i$ is the operator, canonically conjugate to the phase operator θ_i , representing the deviation of the number of Cooper pairs from a constant integer value. The effective capacitance to the ground of each grain C is assumed to be spatially uniform, for simplicity. The second term in (1) is the Josephson-junction coupling between nearest-neighbor grains described by phase variables θ_i and phase shifts A_{ij} . The model in Eq. (1) can also be regarded as a quantum rotor model [36] with the additional effects of quenched gauge disorder. We consider four different quantum rotor models: a gauge- and a flux-glass model [14,16,32,33] with spatial randomness in A_{ij} and a binary and Gaussian phase-glass model [13] with spatial randomness in E_{ij} including $E_{ij} < 0$. The phase-glass model can also be regarded as a quantum version of the chiral-glass model [7,37,38] used to study the thermal phase transition in the absence of charging effects.

For the gauge- and flux-glass models, A_{ij} represents the line integral of the vector potential $A_{ij} = \frac{2\pi}{\Phi_0} \int_i^j \mathbf{A} \cdot d\mathbf{l}$, due to an external magnetic field $\mathbf{B} = \nabla \times \mathbf{A}$. For the *gauge-glass model*, we set $E_{ij} = E_J$ (uniform) and choose A_{ij} as a random variable uniformly distributed in the interval $[-\pi, \pi]$ but uncorrelated in space. It may describe, for example, the limit of very large disorder in the positions of the superconducting grains. In the *flux-glass model*, the variation of the magnetic flux $\delta f_p = B\delta S_p/\Phi_0$ in a plaquette of area S_p , in units of the flux quantum $\Phi_0 = hc/2e$, is the spatially uncorrelated random variable, which we choose to be uniform in the interval $[-1, 1]$. This could represent a large disorder in the size of the grains, which induces uncorrelated variations in the magnetic flux at different plaquettes or randomness in the plaquette areas. The flux-glass model can also be regarded as a gauge-glass model with a particular long-range correlated disorder [32,33] in A_{ij} . The *phase-glass model* describes the effects of disorder in E_{ij} due to the random location of negative Josephson coupling ($E_{ij} < 0$). In this case, we set $A_{ij} = 0$ and choose $E_{ij} = \pm E_J$, with equal probability (binary distribution) or with probability $P(E_{ij}) = e^{-E_{ij}^2/2E_J^2}/E_J\sqrt{2\pi}$ (Gaussian distribution). Since $E_{ij} < 0$ with $A_{ij} = 0$ is equivalent to a positive Josephson coupling $|E_{ij}|$ with a phase shift $A_{ij} = \pi$, the binary phase-glass model can also be regarded as a gauge-glass model with a binary distribution of phase shifts $A_{ij} = 0$ or π .

The quantum phase transition at zero temperature can be conveniently studied in the framework of the imaginary-time path-integral formulation of the model [39]. In this representation, the two-dimensional (2D) quantum model of Eq. (1) maps

into a (2+1)D classical statistical mechanics problem. The extra dimension corresponds to the imaginary-time direction. Dividing the time axis τ into slices $\Delta\tau$, the ground-state energy corresponds to the reduced free energy F of the classical model per time slice. The classical reduced Hamiltonian can be written as [19,35,39]

$$H = -\frac{1}{g} \left[\sum_{\tau,i} \cos(\theta_{\tau,i} - \theta_{\tau+1,i}) + \sum_{\langle ij \rangle, \tau} e_{ij} \cos(\theta_{\tau,i} - \theta_{\tau,j} - A_{ij}) \right], \quad (2)$$

where $e_{ij} = E_{ij}/E_J$, and τ labels the sites in the discrete time direction. The ratio $g = (E_C/E_J)^{1/2}$, which drives the SI transition for the model of Eq. (1), corresponds to an effective “temperature” in the 3D classical model of Eq. (2). The particular form of the coupling of the phases $\theta_{\tau,j}$ in the time direction results from a Villain approximation, used to obtain the phase representation of the first term in Eq. (1). This approximation, however, should preserve the universal aspects of the critical behavior [39]. In general, a quantum phase transition shows intrinsic anisotropic scaling, with different diverging correlation lengths ξ and ξ_τ in the spatial and imaginary-time directions, respectively, related by the dynamic critical exponent z as $\xi_\tau \propto \xi^z$. The classical Hamiltonian of Eq. (2) can be viewed as a three-dimensional (3D) layered XY model, where frustration effects exist only in the 2D layers. Randomness in e_{ij} or A_{ij} corresponds to disorder completely correlated in the time direction.

Equilibrium Monte Carlo (MC) simulations are carried out using the 3D classical Hamiltonian in Eq. (2) regarding g as a “temperaturelike” parameter. The parallel tempering method [40] is used in the simulations with periodic boundary conditions, as in previous work [16,31]. The finite-size scaling analysis is performed for different linear sizes L of the square lattice with the constraint $L_\tau = aL^z$, where a is a constant aspect ratio. This choice simplifies the scaling analysis; otherwise an additional scaling variable L_τ/L^z would be required to describe the scaling functions. The value of a is chosen to minimize the deviations of aL^z from integer numbers. However, this requires one to know the value of the dynamic exponent z in advance. Since the exact value of z is not known, we follow a two-step approach. First, we obtain an estimate of g_c and z from simulations performed with a *driven* MC dynamics method, which has been used in the context of the 3D classical XY spin-glass model [38]. Then, these initial estimates are improved by finding the best data collapse for the finite-size behavior of the phase stiffness in the time direction γ_τ , obtained by the equilibrium MC method.

For the driven MC method, the layered honeycomb model of Eq. (2) is viewed as a 3D superconductor, and the corresponding “current-voltage” scaling near the transition is used to determine the critical coupling and critical exponents [37]. In the presence of an external driving perturbation J_x (“current density”), which couples to the phase difference $\theta_{\tau,i+\hat{x}} - \theta_{\tau,i}$ along the \hat{x} direction, the classical Hamiltonian of Eq. (2) is modified to

$$H_J = H - \sum_{i,\tau} \frac{J_x}{g} (\theta_{\tau,i+\hat{x}} - \theta_{\tau,i}). \quad (3)$$

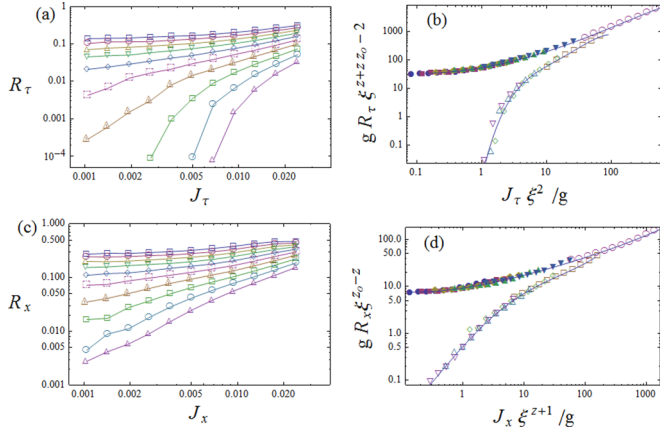


FIG. 1. Scaling behavior of the phase slippage response for the gauge-glass model in (a) the imaginary-time direction R_τ and (c) spatial direction R_x near the SI transition. From the top down, the couplings are $g = 1.75, 1.73, 1.71, 1.69, 1.67, 1.65, 1.63, 1.61, 1.59$, and 1.57 . (b, d) Scaling plots corresponding to (a) and (c), respectively, for data near the transition with $\xi = |g/g_c - 1|^{-\nu}$ using the same parameters $g_c = 1.645$, $z_o = 2.3$, $z = 1.2$, and $\nu = 0.9$.

The MC simulations are carried out using the Metropolis algorithm, and the time dependence is obtained from the MC time t_{mc} . When $J_x \neq 0$, the system is out of equilibrium since the total energy is unbounded. The lower energy minima occur at phase differences $\theta_{\tau,i+\hat{x}} - \theta_{\tau,i}$, which increase with time t_{mc} , leading to a net phase slippage rate proportional to $V_x = \langle d(\theta_{\tau,i+\hat{x}} - \theta_{\tau,i})/dt_{mc} \rangle$, corresponding to the average “voltage” per unit length. The measurable quantity of interest is the phase slippage response (nonlinear resistivity) defined as $R_x = V_x/J_x$. Similarly, we define R_τ as the phase slippage response to the applied perturbation J_τ in the layered (imaginary-time) direction. Above the phase-coherence transition, $g > g_c$, R_x should approach a nonzero value when $J_x \rightarrow 0$, while it should approach zero below the transition. From the nonlinear scaling behavior near the transition of a sufficiently large system, one can extract the critical coupling g_c and the critical exponents ν and z .

III. NUMERICAL RESULTS AND DISCUSSION

A first estimate of the critical coupling g_c and dynamical exponent z can be obtained using the driven MC dynamics method presented in Sec. II for large system sizes. We illustrate the method for the gauge-glass model. Figure 1 shows the behavior of the nonlinear phase slippage response R_x and R_τ for the gauge-glass model as a function of the applied perturbation J_x and J_τ , respectively. The behavior for different values of g is consistent with a phase-coherence transition at an apparent critical coupling in the range $g_c \approx 1.63$ – 1.67 . For $g > g_c$, both R_x and R_τ tend to a finite value while for $g < g_c$, they extrapolate to low values. Assuming the transition is continuous, the nonlinear response behavior sufficiently close to the transition should satisfy a scaling form in terms of J_x , J_τ , and g . The critical coupling g_c and critical exponents ν and z can then be obtained from the best data collapse satisfying the scaling behavior close to the transition. Details of the scaling theory can be found in Ref. [41]. R_x and R_τ should satisfy the

scaling forms

$$\begin{aligned} g R_x \xi^{z_0-z} &= F_\pm(J_x \xi^{z+1}/g), \\ g R_\tau \xi^{z+z_0-2} &= H_\pm(J_\tau \xi^2/g), \end{aligned} \quad (4)$$

where z_o is an additional critical exponent describing the MC relaxation times, $t_{mc,x}^r \approx \xi^{z_o}$ and $t_{mc,\tau}^r \approx \xi_\tau^{z_o}$, in the spatial and imaginary-time directions, respectively, and $\xi = |g/g_c - 1|^{-\nu}$. The + and – signs correspond to $g > g_c$ and $g < g_c$, respectively. The two scaling forms are the same when $z = 1$, corresponding to isotropic scaling. The joint scaling plots according to Eqs. (4) are shown in Figs. 1(b) and 1(d), obtained by adjusting the unknown parameters, providing the estimates $g_c = 1.645$, $z_o = 2.3$, $z = 1.2$, and $\nu = 0.9$.

To obtain the estimates above, it was implicitly assumed that the system is sufficiently large and the coupling parameter is not too close to g_c , allowing the finite-size effects to be neglected. Having obtained an estimate of z , we can now consider the finite-size behavior of the phase stiffness in the imaginary-time direction γ_τ , using equilibrium MC simulations, and improve the determination of g_c and ν . The phase stiffness γ_τ , which is a measure of the free energy cost to impose an infinitesimal phase twist in the time direction, is given by [42]

$$\gamma_\tau = \frac{1}{L^2 L_\tau g^2} [g \langle \epsilon_\tau \rangle - \langle I_\tau^2 \rangle + \langle I_\tau \rangle^2]_D, \quad (5)$$

where $\epsilon_\tau = \sum_{\tau,i} \cos(\theta_{\tau,i} - \theta_{\tau,i+1})$ and $I_\tau = \sum_{\tau,i} \sin(\theta_{\tau,i} - \theta_{\tau,i+1})$. In Eq. (5), $\langle \dots \rangle$ represents a MC average for a fixed disorder configuration and $[\dots]_D$ represents an average over different disorder configurations. In the superconducting phase γ_τ should be finite, reflecting the existence of phase coherence, while in the insulating phase it should vanish in the thermodynamic limit. For a continuous phase transition, γ_τ should satisfy the finite-size scaling form

$$\gamma_\tau L^{2-z} = F(L^{1/\nu} \delta g), \quad (6)$$

where $F(x)$ is a scaling function and $\delta g = g - g_c$. This scaling form implies that data for $\gamma_\tau L^{2-z}$ as a function of g , for different system sizes L , should cross at the critical coupling g_c . Figure 2(a) shows this crossing behavior obtained near the initial estimate of g_c obtained from Fig. 1 by varying slightly g_c and ν from their initial values. In the Inset of this figure, we show a scaling plot of the data according to the scaling form of Eq. (6), which provides for the gauge-glass model the final estimates $g_c = 1.649$ and $\nu = 0.99$. The same value of the dynamic exponent $z = 1.2$ found for the gauge-glass model also gave consistent results for the other models. Figures 3 and 4 show the scaling behavior of the phase stiffness for the flux and binary phase-glass model. We then obtain the estimates $g_c = 1.629$ and $\nu = 0.92$ (flux glass), $g_c = 1.58$ and $\nu = 1.15$ (binary phase glass), $g_c = 1.44$ and $\nu = 1.12$ (Gaussian phase glass).

The SI transition can be further characterized by the behavior of the finite-size correlation length, which can be defined as [43]

$$\xi(L, g) = \frac{1}{2 \sin(k_0/2)} [S(0)/S(k_0) - 1]^{1/2}. \quad (7)$$

Here $S(k)$ is the Fourier transform of the correlation function $C(r)$, and k_0 is the smallest nonzero wave vector.

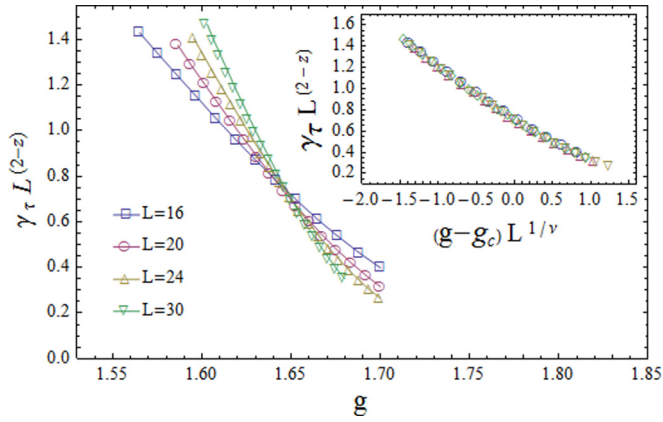


FIG. 2. Phase stiffness in the imaginary-time direction γ_τ for the gauge-glass model with different system sizes L , near the transition point estimated from Fig. 1. $L_\tau = aL^z$, with aspect ratio $a = 0.642$ and $z = 1.2$. Inset: scaling plot of γ_τ with $g_c = 1.649$ and $\nu = 0.99$.

For $g > g_c$, this definition corresponds to a finite-difference approximation to the infinite system correlation length $\xi(g)^2 = -\frac{1}{S(k)} \frac{\partial S(k)}{\partial k^2} |_{k=0}$, taking into account the lattice periodicity. For the random-gauge models considered here, it is convenient to define the correlation function in terms of the overlap order parameter [44] $q_{\tau,j} = \exp[i(\theta_{\tau,j}^1 - \theta_{\tau,j}^2)]$, where 1 and 2 label two different copies of the system with the same coupling parameters. The correlation function in the spatial direction is obtained as

$$C(r) = \frac{1}{L^2 L_\tau} \sum_{\tau,j} \langle q_{\tau,j} q_{\tau,j+r} \rangle, \quad (8)$$

and the analogous expression is used for the correlation function $C_\tau(r)$ in the time direction. For a continuous transition, $\xi(L, g)$ should satisfy the scaling form

$$\xi/L = F(L^{1/\nu} \delta g), \quad (9)$$

where $F(x)$ is a scaling function. Figures 5 and 6 show the behavior of the correlation length ξ_τ and ξ in the time and spatial directions, for the gauge-glass model. The curves for ξ_τ/L as a function of g for different system sizes cross at the same point, providing further evidence of a continuous

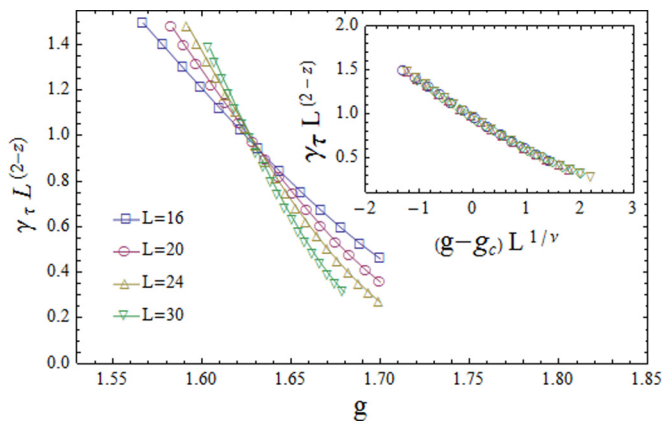


FIG. 3. Same as Fig. 2 but for the flux-glass model. Inset: Scaling plot of γ_τ with $g_c = 1.6294$ and $\nu = 0.92$.

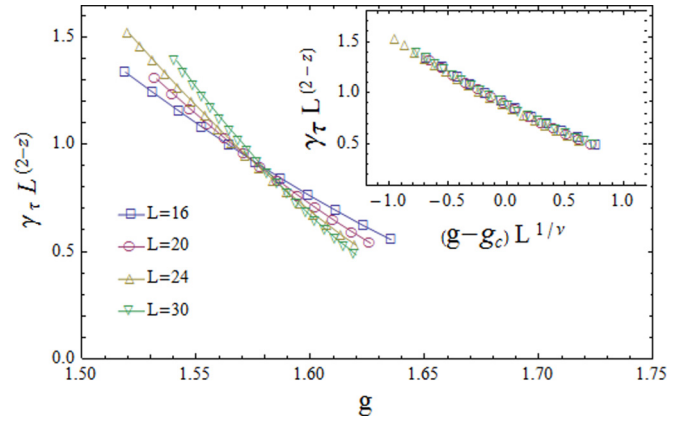


FIG. 4. Same as Fig. 2 but for the phase-glass model. Inset: Scaling plot of γ_τ with $g_c = 1.58$ and $\nu = 1.15$.

transition. In the inset of Fig. 5, a scaling plot according to Eq. (9) is shown, which gives an alternative estimate of $g_c = 1.646$ and $\nu = 1.08$. For the correlation length in the spatial direction shown in Fig. 6 and the corresponding scaling plot, we obtain $g_c = 1.629$ and $\nu = 1.12$. Since in this case the crossing point is less clear, these estimates are more affected by corrections to finite-size scaling. For the flux- and phase-glass models the differences of the estimate of g_c from the correlation in the time and spatial directions are much larger. We consider that the results obtained from the scaling of the phase stiffness γ_τ are more accurate and use them to obtain the final result and the associated error bar.

We have also determined the universal conductivity at the critical point from the frequency and finite-size dependence of the phase stiffness $\gamma(w)$ in the spatial direction, following the scaling method described by Cha *et al.* [36,42]. The conductivity is given by the Kubo formula

$$\sigma = 2\pi\sigma_Q \lim_{w_n \rightarrow 0} \frac{\gamma(iw_n)}{w_n}, \quad (10)$$

where $\sigma_Q = (2e)^2/h$ is the quantum of conductance and $\gamma(iw_n)$ is a frequency-dependent phase stiffness evaluated at

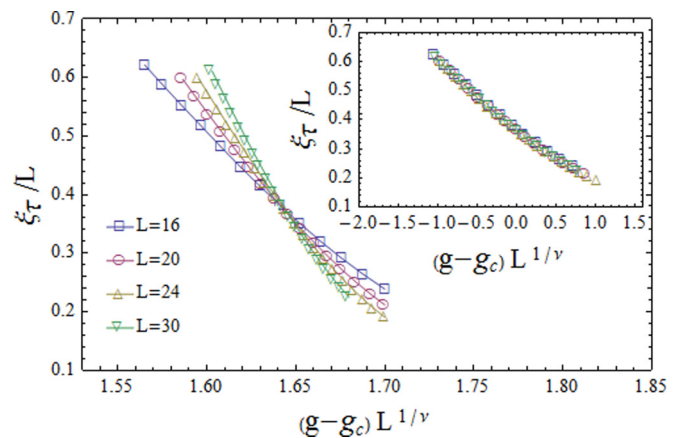


FIG. 5. Correlation length in the imaginary-time direction ξ_τ for the gauge-glass model with different system sizes L . Inset: Scaling plot of ξ_τ with $g_c = 1.646$ and $\nu = 1.08$.

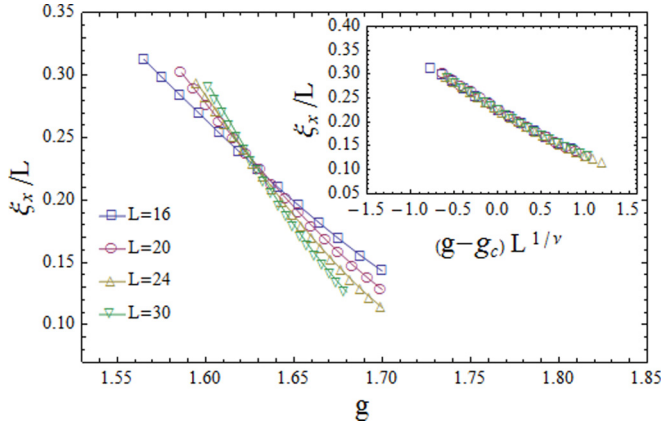


FIG. 6. Correlation length in the spatial direction ξ for the gauge-glass model with different system sizes L . Inset: Scaling plot of ξ with $g_c = 1.629$ and $\nu = 1.12$.

the finite frequency $w_n = 2\pi n/L\tau$, with n an integer. The frequency-dependent phase stiffness in the \hat{x} direction is given by

$$\gamma = \frac{1}{L^2 L_\tau g^2} [g \langle \epsilon_x \rangle - \langle |I(iw_n)|^2 \rangle + \langle |I(iw_n)|^2 \rangle_D], \quad (11)$$

where

$$\begin{aligned} \epsilon_x &= \sum_{\tau,j} e_{i,j+\hat{x}} \cos(\Delta_x \theta_{\tau,j}), \\ I(iw_n) &= \sum_{\tau,j} e_{i,j+\hat{x}} \sin(\Delta_x \theta_{\tau,j}) e^{iw_n \tau}, \end{aligned} \quad (12)$$

and $\Delta_x \theta_{\tau,j} = \theta_{\tau,j} - \theta_{\tau,j+\hat{x}} - A_{j,j+\hat{x}}$. At the transition, $\gamma(iw_n)$ vanishes linearly with frequency and σ assumes a universal value σ^* , which can be extracted from its frequency and finite-size dependence as [42]

$$\frac{\sigma(iw_n)}{\sigma_Q} = \frac{\sigma^*}{\sigma_Q} - c \left(\frac{w_n}{2\pi} - \alpha \frac{2\pi}{w_n L \tau} \right) \dots \quad (13)$$

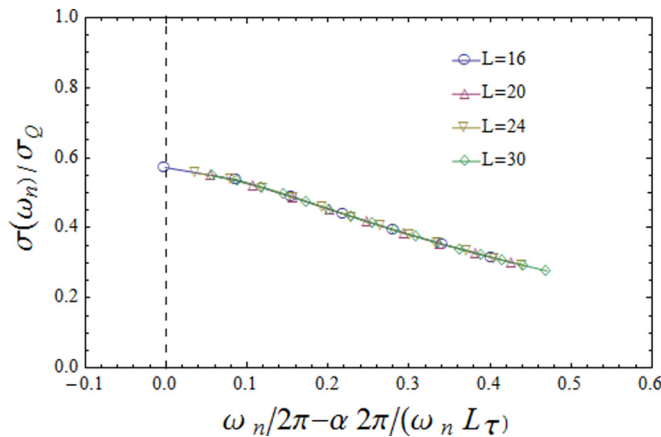


FIG. 7. Scaling plot of conductivity $\sigma(iw_n)$ at the critical coupling g_c for the gauge-glass model with $\alpha = 0.2$. The universal conductivity is given by the intercept with the $x = 0$ dashed line, leading to $\frac{\sigma^*}{\sigma_Q} = 0.56(3)$.

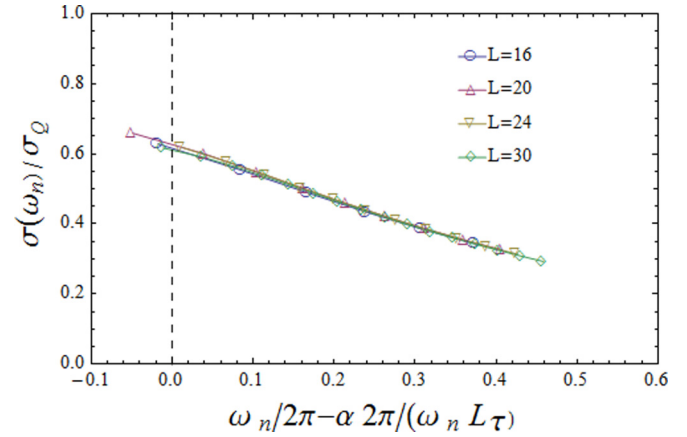


FIG. 8. Same as Fig. 7 but for the flux-glass model with $\alpha = 0.27$. The universal conductivity is given by the intercept with the $x = 0$ dashed line, leading to $\frac{\sigma^*}{\sigma_Q} = 0.61(3)$.

The parameter α is determined from the best data collapse of the frequency-dependent curves for different systems sizes in a plot of $\frac{\sigma(iw_n)}{\sigma_Q}$ versus $x = \left(\frac{w_n}{2\pi} - \alpha \frac{2\pi}{w_n L \tau} \right)$. The universal conductivity is obtained from the intercept of these curves with the line $x = 0$. The calculations were performed for different system sizes with $L\tau = aL^z$, using the above estimates of z and g_c . From the scaling behavior in Fig. 7 we obtain for the gauge-glass model $\sigma^*/\sigma_Q = 0.56(3)$, where the estimated uncertainty is mainly the result of the error in the coupling g_c . Figures 8 and 9 show the behavior for the flux and binary phase-glass models. We then obtain $\sigma^*/\sigma_Q = 0.61(3)$ (flux glass), $\sigma^*/\sigma_Q = 0.60(3)$ (binary phase glass), and $\sigma^*/\sigma_Q = 0.57(3)$ (Gaussian phase glass).

The results for the critical properties of the different random gauge models are summarized in Table I, together with the known values for the pure model. We now compare them with available numerical work and experimental data. The value of the universal conductivity found in the earlier work on the gauge-glass model [14], $\frac{\sigma^*}{\sigma_Q} = 1.06(9)$, differs significantly from our result but the critical exponent $z = 1.3(1)$ is con-

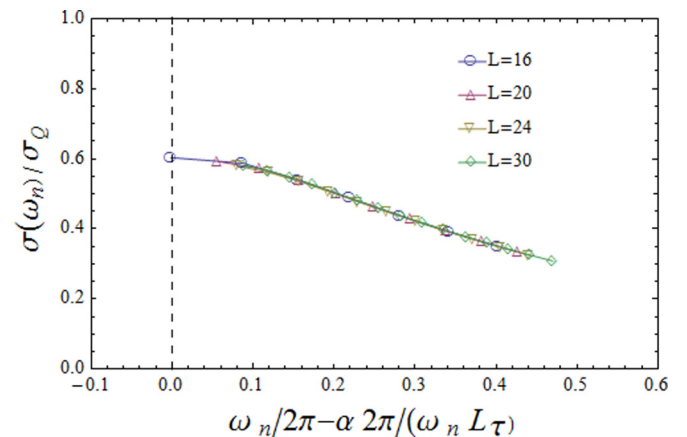


FIG. 9. Same as Fig. 7 but for the binary phase-glass model with $\alpha = 0.06$. The universal conductivity is given by the intercept with the $x = 0$ dashed line, leading to $\frac{\sigma^*}{\sigma_Q} = 0.60(3)$.

TABLE I. Critical exponents z, ν and critical conductivity σ^* for different random gauge models and the pure model (without disorder). g_c is the critical value of the coupling parameter $g = (E_c/E_J)^{1/2}$. The results for the pure case are taken from Ref. [36].

	Pure	Gauge glass	Flux glass	Binary phase glass	Gaussian phase glass
g_c	2.203	1.649(1)	1.629(1)	1.580(5)	1.440(5)
z	1	1.2(1)	1.2(1)	1.2(1)	1.2(1)
ν	0.67	0.99(4)	0.92(4)	1.15(6)	1.12(4)
σ^*/σ_Q	0.29(2)	0.56(3)	0.61(3)	0.60(3)	0.57(3)

sistent with our estimate. The discrepancy in the value of σ^* is mainly due to the different estimate of the critical coupling, $g_c \approx 1.587$, which was obtained by a scaling analysis of the dimensionless ratio of the overlap order parameter $q_{\tau,j}$. This type of “Binder ratio,” however, is not very reliable for models with continuous symmetry [45]. Since our estimate of g_c is based on the scaling behavior of the phase stiffness, which is also consistent with the behavior of the correlation length, we believe it should be more accurate. A different calculation of the critical exponents [15] found $\nu \approx 0.73$ and estimate $z = 1.17(7)$, also compatible with our result for z .

The results for the gauge- and flux-glass models can be compared with experimental observations of the SI transition on thin superconducting films with a pattern of nanoholes [20,24,25]. A minimal model describing phase coherence in these systems consists of a Josephson-junction array defined on an appropriate lattice, with the nanoholes corresponding to the dual lattice [16,30,31]. Very recently [24,25], the effect of a controlled amount of gauge disorder on the SI transition was investigated by introducing geometrical disorder in the form of randomness in the position of the nanoholes. This leads to disorder in the magnetic flux $\delta f_p = B\delta S_p/\Phi_o$ in a plaquette of area S_p , which increases with the applied magnetic field and degree of geometrical disorder. Magnetoresistance oscillations near the SI transition, resulting from commensurate vortex-lattice states, are observed below a critical disorder strength [24] $\delta f_c \approx 0.3$. Although the resistivity at successive field-induced SI transitions varies below this critical disorder, it seems to reach a constant value, independent of the critical coupling for larger disorder [25]. Recent numerical simulations of a Josephson-junction array model suggests that the large disorder regime should correspond to a vortex glass [16]. The gauge- and flux-glass models considered here should then provide the simplest description in this limit. For weak geometrical disorder, the nanoholes form a triangular lattice [20] and therefore the appropriate geometry for the array model should be a honeycomb lattice [16,46]. In the large disorder limit, however, the lattice geometry should not be relevant. In fact, the numerical results for the conductivity at the transition found for a flux-glass model using a honeycomb lattice in the large disorder limit [16] is the same, within the estimated error bar, as found in the present work for the square lattice. In particular, the value of conductivity at the transition found in the experiments for large gauge disorder [24,25] is a factor of 2 larger compared with measurements on samples without an applied magnetic field [20]. This

ratio of the critical conductivities agrees with the results for the gauge- or flux-glass models compared with the pure model in Table I. Therefore, although the magnitudes of the experimental and numerical results are different, the trend of increasing critical conductivity with gauge disorder is correctly given by the gauge- and flux-glass models. Notice, however, that the opposite trend can occur when comparing the large gauge disorder limit with the pure system in the presence of a magnetic field [16]. Moreover, the agreement of the critical properties obtained from the gauge- and flux-glass models and the previous calculations for large disorder from a model on a honeycomb lattice [16] strongly support the experimental observation [25] that the critical conductivity is independent of the coupling parameter in the large disorder limit.

It may appear somehow surprising that the critical conductivity for the phase-glass model is essentially the same as for the gauge-glass model. The phase-glass model has an additional reflection symmetry property [7], where changing $\theta_i \rightarrow -\theta_i$ leaves the Hamiltonian unchanged, whereas for the gauge-glass model there is only a continuous symmetry. One could then expect different universality classes. In the absence of quantum fluctuations, $E_c = 0$, this happens to be the case. In 2D, the transition for increasing temperatures can be described as a thermal transition with vanishing critical temperature, $T_c = 0$, and a divergent thermal correlation length $\xi_T \propto T^{-\nu_T}$. In fact, the values of ν_T for the gauge- and phase-glass models are quite different [9,47]. On the other hand, the SI transition at zero temperature is actually described by an effective $(2+1)$ D classical model [Eq. (2)], with gauge disorder completely correlated in one direction. Interestingly, numerical results for the 3D gauge- and phase-glass models show the same critical exponents [37,38,48], within the estimated error bar, although such calculations have only been carried out for models with uncorrelated disorder.

IV. CONCLUSIONS

We studied the superconductor-insulator transition in two-dimensional inhomogeneous superconductors with gauge disorder, described by four different models: a gauge-glass, a flux-glass, a binary phase-glass, and Gaussian phase-glass model. The first two models describe the combined effect of geometrical disorder in the array of local superconducting islands and a uniform external magnetic field, while the last two describe the effects of randomness in the Josephson couplings alone, allowing for negative couplings. We found that the gauge- and flux-glass models display the same critical behavior, within the estimated uncertainties, and similar behavior is observed for binary and Gaussian phase-glass models. The value of the conductivity at the transition is a factor of 2 larger than for the pure model, which agrees with recent experiments on nanohole thin-film superconductors [24,25] in the large disorder limit, which can be modeled by the gauge- or flux-glass models. This agreement, together with previous results for large disorder from a model on a honeycomb lattice [16], strongly supports the experimental observation [25] that the critical conductivity is independent of the coupling parameter in the large disorder limit, consistent with the scenario of a universal value in this limit. For a more realistic description of these systems, dissipation effects [28], which have been neglected in the

present models, should also be taken into account. It should be noted that the phase-glass models considered here, which show a direct superconductor-to-insulator transition, have a zero mean distribution of Josephson couplings. For a nonzero mean, an analytical work [13] has proposed an intermediate metallic phase (a Bose metal) separating the superconducting and insulating phases.

ACKNOWLEDGMENTS

The author thanks J. M. Valles, Jr., and J. M. Kosterlitz for helpful discussions. This work was supported by CNPq (Conselho Nacional de Desenvolvimento Científico e Tecnológico) in Brazil and computer facilities from CENAPAD-SP.

-
- [1] M. P. A. Fisher, *Phys. Rev. Lett.* **62**, 1415 (1989).
 [2] D. A. Huse and H. S. Seung, *Phys. Rev. B* **42**, 1059 (1990).
 [3] L. Bulaevskii, V. Kuzii, and A. Sobyenin, *JETP Lett.* **25**, 290 (1977).
 [4] B. I. Spivak and S. A. Kivelson, *Phys. Rev. B* **43**, 3740 (1991).
 [5] M. Sgrist and T. M. Rice, *Rev. Mod. Phys.* **67**, 503 (1995).
 [6] F. V. Kusmartsev, *Phys. Rev. Lett.* **69**, 2268 (1992).
 [7] H. Kawamura, *J. Phys. Soc. Jpn.* **64**, 711 (1995).
 [8] H. Kawamura and M. S. Li, *Phys. Rev. Lett.* **78**, 1556 (1997).
 [9] E. Granato, *Phys. Rev. B* **58**, 11161 (1998).
 [10] F. Hrahsheh and T. Vojta, *Phys. Rev. Lett.* **109**, 265303 (2012).
 [11] D. M. Basko and F. W. J. Hekking, *Phys. Rev. B* **88**, 094507 (2013).
 [12] G. Rastelli, M. Vanevi, and W. Belzig, *New J. Phys.* **17**, 053026 (2015).
 [13] P. Phillips, *Science* **302**, 243 (2003).
 [14] K. Kim and D. Stroud, *Phys. Rev. B* **78**, 174517 (2008).
 [15] L.-H. Tang and Q.-H. Chen, *J. Stat. Mech.: Theor. Exp.* (2008) P04003.
 [16] E. Granato, *Phys. Rev. B* **94**, 060504(R) (2016).
 [17] M. P. A. Fisher, G. Grinstein, and S. M. Girvin, *Phys. Rev. Lett.* **64**, 587 (1990).
 [18] M. P. A. Fisher, *Phys. Rev. Lett.* **65**, 923 (1990).
 [19] M. Wallin, E. S. Sorensen, S. M. Girvin, and A. P. Young, *Phys. Rev. B* **49**, 12115 (1994).
 [20] M. D. Stewart, Jr., A. Yin, J. M. Xu, and J. M. Valles, Jr., *Science* **318**, 1273 (2007).
 [21] M. D. Stewart, Jr., A. Yin, J. M. Xu, and J. M. Valles, Jr., *Phys. Rev. B* **77**, 140501 (2008).
 [22] T. I. Baturina, V. M. Vinokur, A. Y. Mironov, N. M. Chitchev, D. A. Nasimov, and A. V. Latyshev, *Europhys. Lett.* **93**, 47002 (2011).
 [23] G. Kopnov, O. Cohen, M. Ovidia, K. H. Lee, C. C. Wong, and D. Shahar, *Phys. Rev. Lett.* **109**, 167002 (2012).
 [24] H. Q. Nguyen, S. M. Hollen, J. M. Valles, Jr., J. Shainline, and J. M. Xu, *Phys. Rev. B* **92**, 140501(R) (2015).
 [25] H. Q. Nguyen, S. M. Hollen, J. M. Valles, Jr., J. Shainline, and J. Xu, *Sci. Rep.* **6**, 38166 (2016).
 [26] H. S. J. van der Zant, L. J. Geerligs, and J. E. Mooij, *Europhys. Lett.* **19**, 541 (1992).
 [27] C. D. Chen, P. Delsing, D. B. Haviland, Y. Harada, and T. Claeson, *Phys. Rev. B* **51**, 15645 (1995).
 [28] R. Fazio and H. van der Zant, *Phys. Rep.* **355**, 235 (2001).
 [29] Z. Han, A. Allain, H. Arjmandi-Tash, K. Tikhonov, M. Feigel'man, B. Sacépé, and V. Bouchiat, *Nat. Phys.* **10**, 380 (2014).
 [30] E. Granato, *Phys. Rev. B* **87**, 094517 (2013).
 [31] E. Granato, *Eur. Phys. J. B* **89**, 68 (2016).
 [32] E. Granato and J. M. Kosterlitz, *Phys. Rev. B* **33**, 6533(R) (1986).
 [33] E. Granato and J. M. Kosterlitz, *Phys. Rev. Lett.* **62**, 823 (1989).
 [34] M. G. Forrester, H. J. Lee, M. Tinkham, and C. J. Lobb, *Phys. Rev. B* **37**, 5966(R) (1988).
 [35] R. M. Bradley and S. Doniach, *Phys. Rev. B* **30**, 1138 (1984).
 [36] M.-C. Cha, M. P. A. Fisher, S. M. Girvin, M. Wallin, and A. P. Young, *Phys. Rev. B* **44**, 6883 (1991).
 [37] C. Wengel and A. P. Young, *Phys. Rev. B* **56**, 5918 (1997).
 [38] E. Granato, *Phys. Rev. B* **69**, 144203 (2004).
 [39] S. L. Sondhi, M. Girvin, J. Carini, and D. Sahar, *Rev. Mod. Phys.* **69**, 315 (1997).
 [40] K. Hukushima and K. Nemoto, *J. Phys. Soc. Jpn.* **65**, 1604 (1996).
 [41] K. H. Lee, D. Stroud, and S. M. Girvin, *Phys. Rev. B* **48**, 1233 (1993).
 [42] M.-C. Cha and S. M. Girvin, *Phys. Rev. B* **49**, 9794 (1994).
 [43] H. G. Ballesteros, A. Cruz, L. A. Fernández, V. Martín-Mayor, J. Pech, J. J. Ruiz-Lorenzo, A. Tarancón, P. Téllez, C. L. Ullod, and C. Ungil, *Phys. Rev. B* **62**, 14237 (2000).
 [44] R. N. Bhatt and A. P. Young, *Phys. Rev. B* **37**, 5606 (1988).
 [45] T. Shirakura and F. Matsubara, *Phys. Rev. B* **67**, 100405 (2003).
 [46] E. Granato, *Physica B* (2017), doi:10.1016/j.physb.2017.09.086.
 [47] H. Kawamura and M. Tanemura, *J. Phys. Soc. Jpn.* **60**, 608 (1991).
 [48] L. W. Lee and A. P. Young, *Phys. Rev. Lett.* **90**, 227203 (2003).